CrystEngComm

Accepted Manuscript

ROYAL SOCIETY OF CHEMISTRY

www.rsc.org/crystengcomm

Journal Name

ARTICLE TYPE

Cite this: DOI: 10.1039/xxxxxxxxxx

Flow-Driven Morphology Control in the Cobalt–Oxalate System†

Eszter Tóth–Szeles[a], **Gábor Schuszter**[a], **Ágota Tóth**[a], **Zoltán Kónya**[b], **Dezső Horváth**[*b]

Received Date
Accepted Date

DOI: 10.1039/xxxxxxxxxx

www.rsc.org/journalname

The interaction of spatial concentration gradients with chemical reactions can lead to intricate precipitate patterns. When the density difference between the reactants is sufficient, gravity current forms at the reactive interface and solid particles can sediment along radially oriented thin lines if both nucleation and crystal growth are slow. In this paper, we have studied the flow-driven Co(II)–oxalate system, by pumping cobalt nitrate solution into a thin layer of sodium oxalate solution. The formed precipitate consists of cobalt(II) oxalate tetrahydrate, identified by thermogravimetric and X-ray diffractometric analysis. This simple flow method to maintain the spatial gradients represents a controlled synthesis resulting in microstructures significantly different from those obtained in well-stirred homogeneous experiments.

1 Introduction

The emerging field of chemobrionics focuses on the interaction of spatial gradients with chemical reactions leading to precipitate formations.[1] In classical one-pot reactions the components are well mixed in an effort to maximize the rate of reaction, unlike in natural processes where the presence of these gradients keeps the system sufficiently far from thermodynamic equilibrium allowing the production of structured materials, accompanied by a local decrease in entropy.[2] The biomimetic synthesis of such materials aims to take advantage of the far-from-equilibrium conditions in well-controlled model systems.[3] The inflow of one component of a precipitation reaction from a local source can lead to the formation of a semipermeable membrane separating the inner and outer electrolyte. The pressure increase driven by osmotic flow ruptures the membrane resulting in growing tubular precipitate structures, often termed chemical gardens.[4–7] These studies have helped to understand the role of spatial gradients in the formation of chimney structures at hydrothermal vents[8], and also provided important information on the physical and chemical consequences of compartmentalization regarding the emergence of life.[8,9] At the reactive interface where the two reactants come into contact, the underlying processes, driven by gradient of concentration, pH, and pressure, form an intricate system, however, simplified model studies in confined geometries have been successful in identifying and characterizing the general features of precipitation reactions coupled with transport processes.[10–12]

The presence of spatial gradients can also lead to the formation of precipitation patterns in the absence of membranes: diffusion coupled with precipitation reaction can produce Liesegang bands[13,14] and even spots[15], while fluid flow driven by a gravity current can result in spatial patterns consisting of distinct radially growing lines along which sedimentation occurs[16]. In the latter case a large convection roll develops at the tip of the spreading inner electrolyte with greater density, which leads to strong local mixing creating a zone of supersaturated solution. This is where then nucleation occurs which may result in precipitates with crystalline form and morphology significantly different from those obtained in a homogeneous solution, as shown in the calcium–oxalate[17] and calcium–carbonate[18] systems. Here we investigate the formation of precipitate patterns in the cobalt–oxalate system

† Electronic Supplementary Information (ESI) available. See DOI: 10.1039/b000000x/

[a] *Department of Physical Chemistry and Materials Science, University of Szeged, Aradi Vértanuk tere 1., Szeged, H-6720, Hungary.*

[b] *Department of Applied and Environmental Chemistry, University of Szeged, Rerrich Béla tér 1., Szeged, H-6720, Hungary. Fax: +36-62-645-482; Tel: +36-62-544-614; E-mail: horvathd@chem.u-szeged.hu*

and present how the precipitate pattern evolves and how morphology is affected by the flow.

Transition-metal oxalate biominerals are widely distributed in nature. In bioweathering of rocks,[19] the oxalic acid secreted by lichens can dissolve metal ions from the mineral substrates and produce various metal(II) oxalate precipitates and hence form new minerals along the interface between the lichen and the rock. For different organisms oxalate precipitation is also a pathway of accumulating toxic metal ions: wood-rotting fungi have enzymes producing oxalic acid and therefore can tolerate toxic metals stress by forming insoluble metal oxalates, the microstructure of which shows radial structure.[20] The investigation of synthetic analogues of natural oxalates hence can play an important role in better understanding the toxic metal immobilization processes by precipitation in biological systems.

Cobalt oxalate is also an important precursor, since its thermal decomposition is the most common commercial method to synthesize Co_3O_4 and cobalt powder,[21–23] the former being used as cathode material in alkaline rechargeable batteries, supercapacitors, thin-film magnetic recording media and in the field of heterogeneous catalysis.[23,24] The microstructure of cobalt(II) oxalate is characterized by rod-like morphology in the range of submicrometer and micrometer[21]. Various synthetic methods have been applied in the past to control the morphology of cobalt oxalate: application of surfactants[22], mechanical solid-phase chemical reaction[25], precipitation in a gel medium[26,27], simple homogeneous precipitation[28], microemulsion method[29], or using extremely alkaline conditions[30]. All these approaches have resulted in cobalt oxalate dihydrate with rod like crystalline morphology different in size although at room temperature tetrahydrate can also be synthesized from aqueous solutions.[31,32]

In this work, we reveal how gravity current maintained by spatial gradients gives rise to an unusual precipitate pattern, and how local mixing leads to the appearance of solid cobalt oxalate with morphology inaccessible in one-pot well-mixed homogeneous systems. With theoretical equilibrium calculations we also show that fast complexation precedes the slow precipitate formation, and characterize our final product with thermogravimety and X-ray diffractometry.

2 Theoretical section

The concentration distribution of each component is calculated in the pH-range of 1–14 by solving the component balance equations for cobalt(II) and oxalate ions. In case the solubility products associated with

$$\mathrm{Co(COO)_2(s)} \overset{K_{sp,Ox}}{\rightleftharpoons} \mathrm{Co^{2+} + (COO)_2^{2-}} \quad (1)$$

$$\mathrm{Co(OH)_2(s)} \overset{K_{sp,OH}}{\rightleftharpoons} \mathrm{Co^{2+} + 2OH^-} \quad (2)$$

Table 1 Solubility products and equilibrium constants[33,34] used in the calculations

$pK_{sp,Ox} = 8.57$	$pK_{sp,OH} = 14.6$
$\log_{10} K_{H,1} = 3.55$	$\log_{10} K_{H,2} = 1.04$
$\log_{10} \beta_{Ox,1} = 3.25$	$\log_{10} \beta_{Ox,2} = 5.60$
$\log_{10} \beta_{HOx,1} = 1.61$	$\log_{10} \beta_{HOx,2} = 2.89$
$\log_{10} \beta_1 = 3.78$	$\log_{10} \beta_2 = 8.32$
$\log_{10} \beta_3 = 9.66$	$\log_{10} \beta_4 = 9.54$
$\log_{10} \beta_{21} = 3.10$	

are reached, the amounts of solid precipitate in a unit volume are also taken into account in the balance equations. Cobalt excess is maintained by setting the total concentration of cobalt ($c_{Co,T}$) to 1.0 mol/dm^3 and that of oxalate ($c_{Ox,T}$) to 0.1 mol/dm^3 in the calculations, where pH is adjusted in steps of 10^{-4}. Wolfram Mathematica is used to solve the set of nonlinear equations (see constants in Table 1).

In the liquid phase we consider the complex formation of oxalate and hydroxide according to

$$\mathrm{Co^{2+} + (COO)_2^{2-}} \overset{\beta_{Ox,1}}{\rightleftharpoons} \mathrm{Co(COO)_2(aq)} \quad (3)$$

$$\mathrm{Co(COO)_2(aq) + (COO)_2^{2-}} \overset{\beta_{Ox,2}}{\rightleftharpoons} \mathrm{Co[(COO)_2]_2^{2-}} \quad (4)$$

$$\mathrm{Co^{2+} + HOOC{-}COO^-} \overset{\beta_{HOx,1}}{\rightleftharpoons} \mathrm{Co(HOOC{-}COO)^+} \quad (5)$$

$$\mathrm{Co^{2+} + 2\,HOOC{-}COO^-} \overset{\beta_{HOx,2}}{\rightleftharpoons} \mathrm{Co(HOOC{-}COO)_2} \quad (6)$$

$$\mathrm{Co^{2+} + OH^-} \overset{\beta_1}{\rightleftharpoons} \mathrm{Co(OH)^+} \quad (7)$$

$$\mathrm{Co^{2+} + 2\,OH^-} \overset{\beta_2}{\rightleftharpoons} \mathrm{Co(OH)_2(aq)} \quad (8)$$

$$\mathrm{Co^{2+} + 3\,OH^-} \overset{\beta_3}{\rightleftharpoons} \mathrm{Co(OH)_3^-} \quad (9)$$

$$\mathrm{Co^{2+} + 4\,OH^-} \overset{\beta_4}{\rightleftharpoons} \mathrm{Co(OH)_4^{2-}} \quad (10)$$

$$\mathrm{2\,Co^{2+} + OH^-} \overset{\beta_{21}}{\rightleftharpoons} \mathrm{Co_2(OH)^{3+}} \quad (11)$$

and the protonation processes of oxalate ion via

$$\mathrm{(COO)_2^{2-} + H^+} \overset{K_{H,1}}{\rightleftharpoons} \mathrm{HOOC{-}COO^-} \quad (12)$$

$$\mathrm{HOOC{-}COO^- + H^+} \overset{K_{H,2}}{\rightleftharpoons} \mathrm{(COOH)_2}. \quad (13)$$

The construction of the balance equations then yields

$$c_{Ox,T} = [(COO)_2^{2-}] + [HOOC{-}COO^-] + [(COOH)_2] + [Co(COO)_2(aq)] + [Co(COO)_2(s)] + 2[Co[(COO)_2]_2^{2-}] + [Co(HOOC{-}COO)^+] + 2[Co(HOOC{-}COO)_2] \quad (14)$$

$$c_{Co,T} = [Co^{2+}] + [Co(OH)^+] + [Co(OH)_2(aq)] + [Co(OH)_2(s)] + [Co(OH)_3^-] + [Co(OH)_4^{2-}] + [Co(COO)_2(aq)] + [Co(COO)_2(s)] + [Co[(COO)_2]_2^{2-}] + [Co(HOOC{-}COO)^+] + [Co(HOOC{-}COO)_2] + [Co_2(OH)^{3+}] \quad (15)$$

where the concentration of each species can be expressed as a function of $[OH^-]$, $[Co^{2+}]$, and $[(COO)_2^{2-}]$, while $[Co(COO)_2(s)]$ and $[Co(OH)_2(s)]$ represent the amount of precipitate in a unit volume. For a given pH the numerical solution of the equations provides these concentrations, from which the concentration distribution curve ($\log_{10} c$ vs. pH) is obtained.

3 Experimental section

Sodium oxalate solution (VWR) is poured into a square glass dish with 22 cm-long sides to create a 5 mm thin liquid layer. Cobalt(II) nitrate solution (1–6 mL) is then pumped into the sodium oxalate by a peristaltic pump (Ismatec Reglo) at 5–20 mL/h flow rate from below through an orifice with 0.4 mm inner diameter, which is positioned in the center of the reaction vessel open to air from the top, as shown in Fig. 1. The injection from the bottom represents the smallest perturbation of the flow field as the liquid being pumped in has greater density. The concentration of sodium oxalate is varied between 0.05 and 0.25 mol/dm^3, and the cobalt(II) nitrate solution has a concentration range of 0.1–1.0 mol/dm^3. The density of each solution is measured with an Anton Paar DMA 500 density meter within 10^{-4} g/cm^3 precision, the determined values are shown in the ESI†. Before transferring the liquid into the container, the pH of the sodium oxalate solution is adjusted to 6.25±0.03 by adding nitric acid. The spatial spreading of the precipitate pattern is monitored by a Canon MV901 digital camera and the digitized images are analyzed quantitatively using in-house software. The chemical composition of a 10–15 mg solid precipitate, having rinsed with deionized water and dried at room temperature, is determined by thermogravimetric measurements (MOM Q–1500D) at 5 °C/min heating rate in air and by using a powder X-ray diffractometer (Rigaku Miniflex II) with CuK$_\alpha$ radiation and 2θ scan in the range of 10–60° with a step size of 1°/min. The microstructure of the crystals is observed by a field emission scanning electron microscope (Hitachi S-4700). In addition, 25 cm^3 of sodium oxalate solution is added to cobalt(II) nitrate in a well-stirred batch experiment as a homogeneous reference system. A UV-VIS spectrophotometric study of the early stages of this premixed system, prior to the precipitate formation, is also carried out.

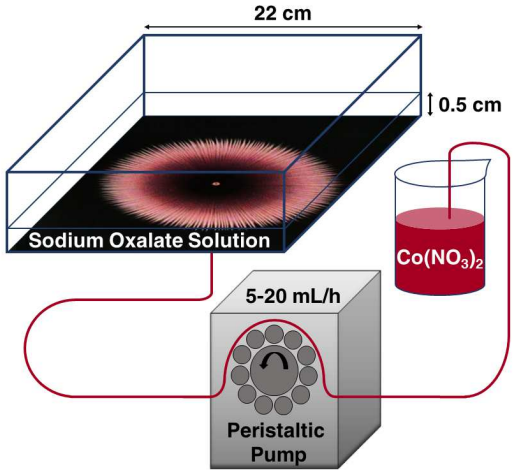

Fig. 1 Schematic drawing of the experimental setup. Into the vessel (22 × 22 cm × 5 cm) containing the oxalate solution (250 mL), 1–6 mL cobalt nitrate solution is pumped in by a peristaltic pump at flow rate 5–20 mL/h.

4 Results and discussion

The concentration distributions of the dominant species are presented in Fig. 2. With cobalt being in excess, oxalate is quantitatively removed from the solution into $Co(COO)_2$ precipitate even at low pH, while the excess cobalt mainly remains in its hydrated ionic form. At pH=6.72, the excess cobalt precipitates out as $Co(OH)_2$ with both solid being present in the system in the pH range of 6.72–10.48. At the upper limit, the entire cobalt(II) oxalate precipitate is transformed into cobalt(II) hydroxide precipitate, liberating the free oxalate ion. In the entire range the oxalato and hydroxo complexes are only present in negligible amount according to the calculations. The same concentration

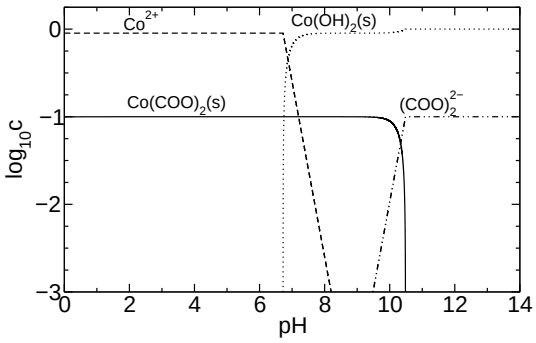

Fig. 2 Concentration distribution of the species as a function of pH.

distribution can be observed with lower oxalate concentration ($c_{Ox,T} = 0.05$ mol/dm^3). The results of the calculations has aided us in setting the initial pH of our system in the experiments where conditions are aimed at the formation of cobalt(II) oxalate precipitate without that of cobalt(II) hydroxide.

In the flow system, as the solution containing the cobalt ion enters the vessel filled with sodium oxalate, it advances along the bottom because of its greater density. This outward spreading does not lead to immediate precipitate formation, instead, at a certain distance from the inlet approximately equidistant lines growing radially evolve, along which precipitate sedimentation occurs as shown in Fig. 3(a) similar to the copper oxalate filaments[16]. As the precipitate pattern grows, the spacing between the filaments increases, since no splitting of the filaments is observed on the time scale of experiments. Except at the lowest

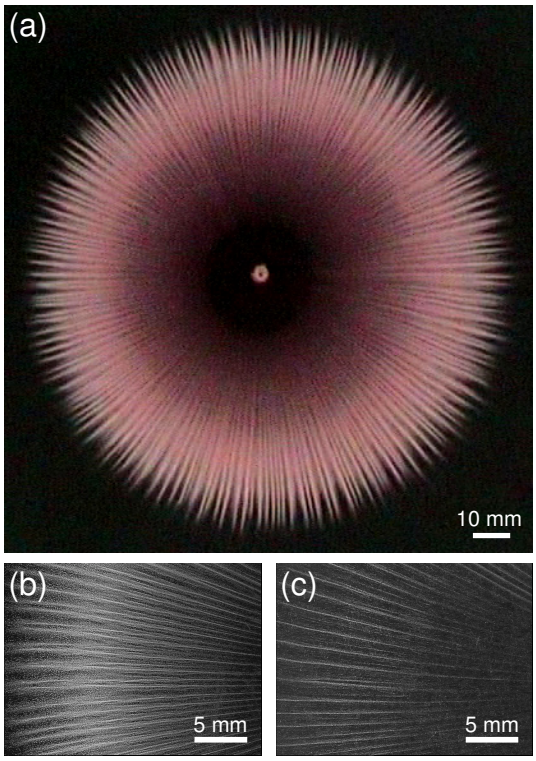

Fig. 3 Cobalt-oxalate precipitate pattern (a) with $[Co^{2+}] = 1$ mol/dm^3, $[Na_2(COO)_2] = 0.1$ mol/dm^3, $Q = 20$ ml/h, $t = 600$ s. Enlargement of the precipitate filaments (b) $[Na_2(COO)_2] = 0.075$ mol/dm^3, $t = 226$ s and (c) $[Na_2(COO)_2] = 0.05$ mol/dm^3, $t = 442$ s.

oxalate concentration, the growing of these precipitate filaments is accompanied by the slower formation of a precipitate ring that may fill the originally transparent space between the lines. This ring formation only becomes more pronounced if the oxalate concentration is increased, cf. Fig. 3(b) and Fig. 3(c). The evolution of the entire precipitate structure initially more or less follows the geometric spreading of the solution entering the container until it stops well before depleting the oxalate solution in the entire container. Beyond this, no significant precipitate formation takes place in the time scale of our experiments. For the qualitative characterization of the precipitation process, we have measured the final diameter of the inner precipitate-free zone (d_i) and the precipitate ring (d_r) and that associated with the tip of the filaments (d). Each diameter is an average of four direct measurements on the image at different locations at a selected time ($t = 520$ s) when the pattern has fully developed. The inner precipitate-free zone is defined as the region with grayscale values corresponding to the background, the outer rim of the precipitate ring is associated with the outer radius of the ring with maximum grayscale, and the tip of the filaments appears as a point of inflection in the grayscale values (see ESI†).

Upon increasing the concentration of sodium oxalate, the diameter of the inner precipitate-free zone decreases monotonously as shown in Fig. 4. This is a result of the greater rate of reaction due to the increased concentration: the precipitate forms faster and hence appears at shorter distance from the center inlet at constant flow rate. Above the critical sodium oxalate concentration (0.075 mol/dm^3) where precipitate ring formation is observed, a similar monotonous shrinking of its diameter occurs with increasing oxalate concentration (see Fig. 4), along with the decrease in the ring width (i.e. $(d_r - d_i)/2$).

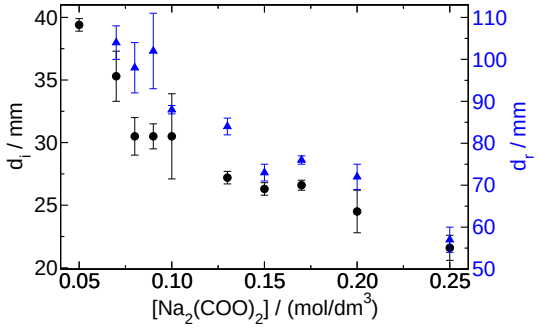

Fig. 4 Diameter of the inner precipitate-free circle (d_i) and the precipitate ring (d_r) as a function of oxalate concentration with $[Co^{2+}] = 1$ mol/dm^3 and $Q = 20$ ml/h.

For oxalate concentrations between 0.05 and 0.25 mol/dm^3, the initially precipitate-free gaps between the radially oriented precipitate filaments increase (2–3 mm) in accordance with the smaller number of filaments (N) appearing in a quarter circle as shown in Fig. 5. The number of the filaments is determined by creating a circular grayscale profile by an in-house software and counting the maxima indicating the location of a filament in the four quarter circles.

This angular variation in the particle density of the precipitate leading to the separation of distinct thin lines rich in precipitate

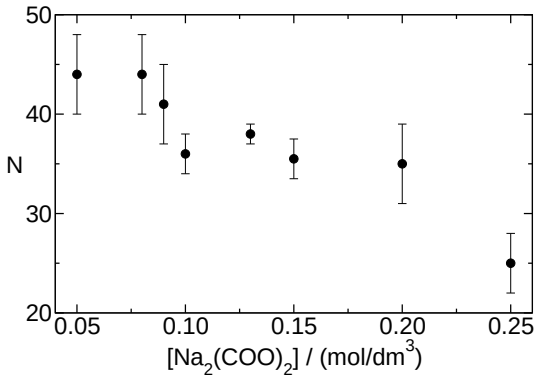

Fig. 5 Number of precipitate filaments at different oxalate concentrations in a quarter circle ($[Co^{2+}] = 1$ mol/dm^3 and $Q = 20$ ml/h).

with precipitate-free gaps between them only arises if the density of the liquid pumped in is sufficiently greater than that of the outer liquid. In this system, a minimum cobalt concentration of 0.18 mol/dm^3 is necessary to obtain the precipitate filaments. Below this critical concentration, only the precipitate ring with homogeneous angular distribution of cobalt oxalate precipitate develops, furthermore, under 0.1 mol/dm^3, no precipitation reaction takes place.

The most favorable condition for the formation of filamental precipitate pattern is achieved at large cobalt ion and small oxalate ion concentration, i.e., when the density difference between the two solutions is at maximum. In this case the gravity current arising at the bottom is the thinnest, representing greater spreading with an average height ($\bar{h}$) of 0.21 mm according to

$$\bar{h} = \frac{V}{A} = \frac{Q\,t}{r^2\,\pi} \tag{16}$$

where $\bar{h}$ is defined as the ratio of the volume pumped in (V) by time t and the visible upper circular surface area (A) at time t; Q is the volume flow rate and $r = d/2$ is the radius of the precipitate pattern at time t. By either increasing the concentration of oxalate ion or decreasing that of cobalt ion leads to smaller density difference, and hence yields precipitate patterns characterized with smaller diameters and less filamental structure. The importance of fluid motion is also supported by the fact that larger pumping rate also favors the filamental pattern with angular variation in the particle density of the precipitate. The small height of the gravity current explains why the characteristics of the precipitate pattern are independent of the liquid height: the precipitate formation occurs at the very bottom of the solution layer with no reaction taking place in the upper region of the liquid.

As the gravity current spreads, the denser solution containing the cobalt ion advances on the bottom forcing the initially stationary oxalate solution upward. This creates a large convection roll at the tip that is responsible for mixing the two components. Super-saturation of cobalt oxalate is therefore only reached locally, around the circular edge of the gravity current. Nucleation and growth of crystals, however, are characterized by slow kinetics not only here in the flow-system, but also in the well-stirred reference experiment, where precipitate formation occurs on the minute scale. The colloidal particles are hence carried back by the reverse flow and phase separation only starts to take place behind the large vortex in a narrow zone where descending and ascending flow alternates transverse to the direction of gravity current. This Rayleigh-Taylor instability is a result of the viscous drag at the bottom, where horizontal fluid velocity is smaller than at the center of the gravity current, giving rise to a region of hydrodynamically unstable stratification with denser liquid on top of less dense. Precipitate sedimentation therefore occurs at the locations of downward flow and precipitate-free gaps indicate those of upward flow, giving rise to the radially growing distinct filaments of the pattern. Pattern formation arises as long as the drag exists at the bottom creating a no-slip boundary condition for fluid flow, hence the same pattern is formed above a plastic bottom surface in the experiments. In systems where both nucleation and crystal growth are fast, phase separation occurs closer to the tip and ahead of the unstable zone, the precipitate pattern will have a disc shape with less distinct filaments, as observed in the calcium-oxalate[17] and calcium–carbonate[18] systems. In a different scenario, dendritic crystal growth is also accompanied by the loss of circular symmetry[37,38], however instead of the buoyancy driven instability, the anisotropy in the growth rates of the various faces and the interfacial tension are the key factors in the symmetry breaking on the smaller length scale, which may for instance lead to the formation of branched fractal patterns.[39]

Unlike the precipitation reaction, complex formation between cobalt and oxalate is instantaneous, only the darker colour of cobalt-oxalate is visible upon the mixing of the two solutions. The systematic spectrophotometric study we have carried out using the Job method indicates that 1:1 complex dominates the system prior to the precipitate appearance. The equilibrium calculations relevant to the precipitate-free solution based on Eqs. (3-11) lead to results in accordance with experimental observation and only predict minor contributions from the dioxalato complex.

Thermal analysis of the solid sample obtained from the precipitate structure reveals that it is the tetrahydrate form of cobalt oxalate.[31,35] The last step in the thermogravimetric measurement shown in Fig. 6 is the conversion to cobalt(II) oxide—the most stable form above 900 °C—according to Eq. (17)

$$2\,Co_3O_4 \longrightarrow 6\,CoO + O_2 \tag{17}$$

The mass of the residue is about 26% of the initial mass, which gives $Co(COO)_2 \cdot 4\,H_2O$ for the chemical composition of cobalt oxalate. The loss of crystallization water takes place in two steps:

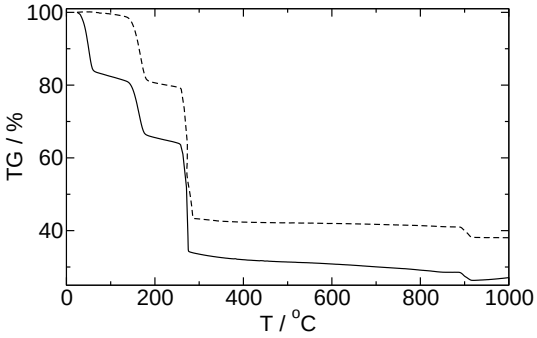

Fig. 6 Thermal decomposition of cobalt-oxalate tetrahydrate (solid line) and dihydrate in flow system (dashed line).

one in the range of 24–60 °C via

$$Co(COO)_2{\cdot}4H_2O \longrightarrow Co(COO)_2{\cdot}2H_2O + 2H_2O \qquad (18)$$

the other in the range of 140–180 °C as

$$Co(COO)_2{\cdot}2H_2O \longrightarrow Co(COO)_2 + 2H_2O \qquad (19)$$

with 18% loss of initial mass. The dehydrated cobalt oxalate starts to decompose at 250 °C, yielding cobalt(II,III) oxide according to

$$3Co(COO)_2 \longrightarrow Co_3O_4 + 4CO + 2CO_2 \qquad (20)$$

The powder diffraction pattern also supports the presence of tetrahydrate form. In Fig. 7(a) the diffraction maxima at $2\theta = 14.8°$ and $2\theta = 16.1°$ distinguish it from the dihydrate form.

The grayish pink cobalt oxalate tetrahydrate isolated from the precipitate pattern in solid state at room temperature dehydrates into the stable bright pink dihydrate form after two days. The transformation not only can be followed visually due to the color change but also is indicated by the change in the thermal decomposition curve, which shows one less steps with mass loss (see dashed lines in Fig. 6), and is supported by the lack of diffraction peaks at 14.8° and 16.1° in Fig. 7(b).[31,35]

The microstructure of the dried precipitate is characterized at two different reactant compositions. The cobalt(II) oxalate tetrahydrate sampled from the precipitate filaments consists of the spherulite polycrystalline particles with diameter $20-50$ μm as seen in Fig. 8(a). This is in contrast to the rod-like crystals with diameter between $10-20$ μm observed in the absence of spatial gradients in the well-stirred reference experiments (see Fig. 8(b)). The slow transition into the dihydrate form does not give rise to a change in the morphology, since both the polycrystalline particles of the flow-system and the rod-like crystals of the well-stirred reference system retain their structure as shown in Fig. 9.

At lower sodium oxalate concentration the rod-like microstructure continues to dominate the precipitate formed in the well-stirred reference experiments as seen in Fig. 10(a). The polycrystalline aggregates arising in the flow system, however, appear less densely packed. An hour-long ultrasonication reveals that the primary particles of these urchin-like spherulite polycrystalline microstructures are 10 μm long rod-like crystals (cf. Fig. 10(b) and (c)).

It is important to point out that the subsequent calcination of the solid sample separated from the precipitate in the flow system in air in order to synthesize cobalt(II) oxide also maintains the morphology, as the final product (CoO) has the same microstructure as the original tetrahydrate isolated from the precipitate pattern (see Fig. 11).

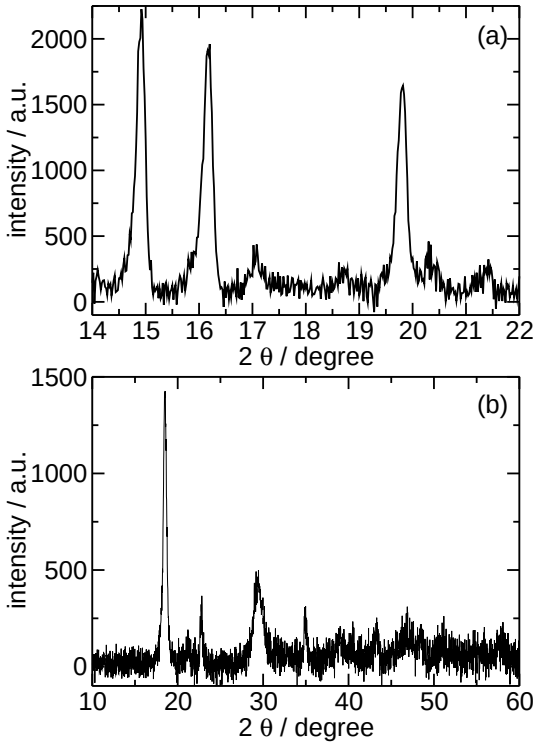

Fig. 7 The powder diffraction pattern of the grayish pink cobalt oxalate tetrahydrate (JCPDS No. 00-037-0534) (a) and after dehydration the bright pink cobalt oxalate dihydrate (JCPDS No. 00-048-1068) (b) with $[Co^{2+}] = 1$ mol/dm^3, $[Na_2(COO)_2] = 0.1$mol/dm^3, $Q = 20$ ml/h

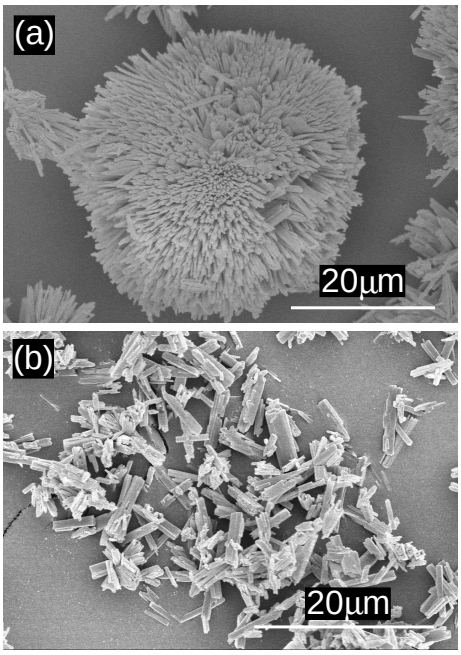

Fig. 8 Spherical polycrystalline particles of cobalt oxalate tetrahydrate (a) that form the radially growing precipitate filaments in the flow system at $[Co^{2+}] = 1$ mol/dm^3 and $[Na_2(COO)_2] = 0.1$ mol/dm^3 with $Q = 20$ ml/h. Also shown are the rod-like crystals obtained in the well-stirred reference experiment (b).

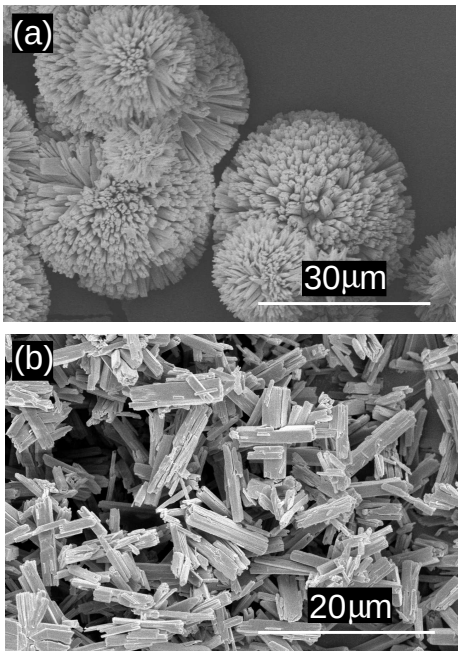

Fig. 9 Cobalt oxalate dihydrate inheriting the morphology of the precursor tetrahydrate: spherical polycrystalline particles from the flow system (a) and the rod-like crystals from the well-stirred reference experiment (b). The experimental conditions are identical to those of Fig. 8.

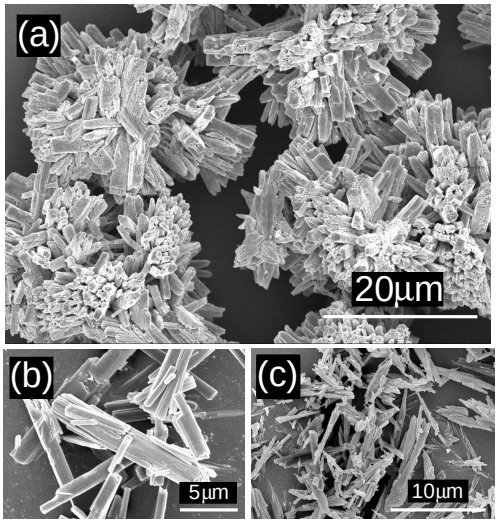

Fig. 10 SEM images of cobalt-oxalate dihydrate microstructure in homogeneous system (a) and in flow system (b) with $[Co^{2+}] = 1$ mol/dm^3, $[Na_2(COO)_2] = 0.05$ mol/dm^3 and $Q = 20$ ml/h. Picture (c) shows the primary particles from the flow system caused by one hour long ultrasonic vibration.

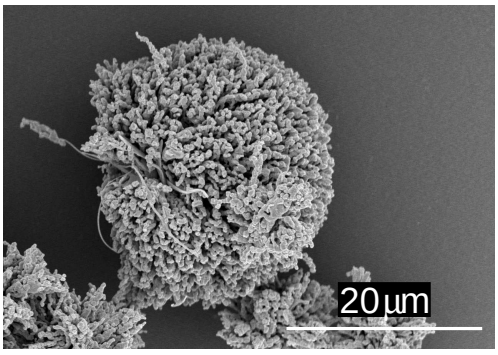

Fig. 11 SEM image of cobalt oxide microstructure prepared from cobalt oxalate tetrahydrate with condition identical to those of Fig. 9

5 Conclusion

In this work we have shown that a gravity current maintained by the inflow of the reactant solution with greater density leads to unusual precipitate pattern formation in the cobalt–oxalate system. We have seen that slow nucleation and crystal growth are essential for the flow to create radially grown lines along which the sedimentation occurs. The local mixing by the convection roll at the tip of gravity current creates the supersaturated zone where the precipitation reaction takes place and the flow provides the influx of fresh reactants. Although the chemical composition is identical to that obtained in the well-stirred reference experiment: cobalt(II) oxalate tetrahydrate, its microstructure is characterized with spherulite polycrystalline aggregates instead of the rod-like crystals of the gradient-free system. The microstructure of the solid material is retained in the subsequent loss of crystallization water. The presence of the fluid flow by maintaining the density gradient and controlling the flow rate hence provides a simple method to modify the microstructure of the solid product in an easy manner.

6 Acknowledgments

This work has been supported by ESA (ESTEC 4000102255/11/NL/KML) and the Hungarian Scientific Research Fund (K112531).

References

1 L. M. Barge, *et al.*, *Chem. Rev.*, 2015, **115**, 8652–8703.
2 *Biomineralization I*, ed. K. Naka, Springer, Berlin, 2007.
3 S. Mann, *Angew. Chem. Int. Ed.*, 2000, **39**, 3392–3406.
4 J. H. E. Cartwright, B. Escribano and C. I. Saniz-Díaz, *Langmuir*, 2011, **27**, 3286–3293.
5 R. Makki and O. Steinbock, *J. Phys. Chem. C*, 2011, **115**, 17046–17053.
6 R. Makki, L. Roszol, J. J. Pagano and O. Steinbock, *Phil. Trans. R. Soc.*, 2012, **370**, 2848–2865.
7 R. Makki, X. Ji, H. Mattoussi and O. Steinbock, *J. Am. Chem. Soc.*, 2014, **136**, 6463–6469.
8 M. Russel, *American Scientist*, 2006, **94**, 32–39.
9 J. Maselko, M. Kiehl, J. Couture, A. Dyonizy, V. Kaminker, P. Nowak and J. Pantaleone, *Langmuir*, 2014, **30**, 5726–5731.
10 F. Haudin, V. Brasiliense, J. H. E. Cartwright, F. Brau and A. De Wit, *Phys. Chem. Chem. Phys.*, 2015, **17**, 12804–12811.
11 F. Haudin, J. H. E. Cartwright and A. De Wit, *J. Phys. Chem. C*, 2015, **119**, 15067–15076.
12 F. Haudin and A. De Wit, *Phys. Fluids*, 2015, **27**, 113101.
13 S. C. Müller and J. Ross, *J. Phys. Chem. A*, 2003, **107**, 7997–8008.
14 I. Lagzi and D. Ueyama, *Chem. Phys. Lett.*, 2009, **468**, 188–192.
15 M. Dayeh, M. Ammar and M. Al-Ghoul, *RSC Adv.*, 2014, **4**, 60034–60038.
16 A. Baker, Á. Tóth, D. Horváth, J. Walkush, A. S. Ali, W. Morgan, Á. Kukovecz, J. J. Pantaleone and J. Maselko, *J. Phys. Chem. A*, 2009, **113**, 8243–8248.
17 B. Bohner. G. Schuszter, O. Berkesi, D. Horváth and Á. Tóth, *Chem. Commun.*, 2014, **50**, 4289–4291.
18 B. Bohner, G. Schuszter, D. Horváth and Á. Tóth, *Chem. Phys. Lett*, 2015, **631**, 114–117.
19 G. M. Gadd, J. Bahri-Esfahani, Q. Li, Y. J. Rhee, Z. Wei, M. Fomina and X. Liang, *Fungal Biology Reviews*, 2014, **28**, 36–55.
20 A. Jarosz-Wilkolazka and G. M. Gadd, *Chemosphere*, 2003, **52**, 541–547.
21 X. Wang, X. Chen, L. Gao, H. Zheng, Z. Zhang and Y. Qian, *J. Phys. Chem. B*, 2004, **108**, 16401–16404.
22 V. Baco-Carles, A. Arnal, D. Poquillon and P. Tailhades, *Powder Technol.*, 2007, **185**, 231–238.
23 D. Wang, Q. Wang and T. Wang, *Inorg. Chem.*, 2011, **50**, 6482–6492.
24 T. E. Karis, X. C. Guo, B. Marchon, V. Raman and Y. L. Hsiao, *IEEE T. Magn.*, 2006, **42**, 2507–2509.
25 Y. Deng, X. Xiong, J. P. Zou, L. Deng and M. J. Tu, *J. Alloy Compd.*, 2015, **618**, 497–503.
26 A. S. Khan, T. C. Devore and W. F. Reed, *J. Cryst. Growth*, 1976, **35**, 337–339.
27 Y. P. Prananto, M. M. Khunur, D. T. Wahyuni, R. A. Shobirin, Y. R. Nata and E. Riskah, *Bull. Chem. React. Eng. Catal.*, 2013, **7**, 198–204.
28 S. Sharma, N. Garg, K. V. Ramanujachary, S. E. Lofland and A. K. Ganguli, *Cryst. Growth Des.*, 2012, **12**, 4202–4210.
29 J. Ahmed, T. Ahmad, K. V. Ramanujachary, S. E. Lofland and A. K. Ganguli, *J. Colloid Interf. Sci.*, 2008, **321**, 434–441.
30 Z. Liu, Z. Liu, Q. Li, T. Yang and D. Zhang, *Mater. Chem. Phys.*, 2011, **131**, 102–107.
31 E. Wisgerhof and J. W. Geus, *Mat. Res. Bull.*, 1983, **18**, 993–1000.
32 E. Wisgerhof and J. W. Geus, *Mat. Res. Bull.*, 1984, **19**, 1591–1598.
33 S. Kotrlý and L. Šůcha, *Handbook of Chemical Equilibria in Analytical Chemistry*, Ellis Horwood Ltd, 1985.
34 L. C. Soare, *Ph.D. dissertation*, 2004.
35 A. Venkataraman, N. V. Sastry and A. Ray, *J. Phys. Chem. Solids*, 1992, **53**, 681–685.
36 P. Pusztai, E. Tóth-Szeles, D. Horváth, Á. Tóth, Á. Kukovecz and Z. Kónya, *Cryst. Eng. Comm.*, 2015, **17**, 8477–8485.
37 M. E. Glicksman and A. O. Lupulescu, *J. Cryst. Growth*, 2004, **264**, 541–549.
38 T. Haxhimali, A. Karma, F. Gonzales and M. Rappaz, *Nat. Mater.*, 2006, **5**, 660–664.
39 V. Fleury, *Nature*, 1997, **390**, 145–148.

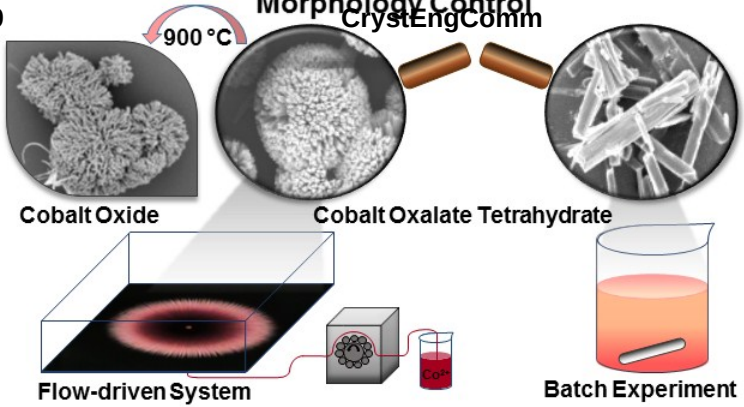

The presence of fluid flow by maintaining the density gradient and controlling the flow rate provides a simple method to modify the microstructure of cobalt oxalate.